Stoichiometry of $Fe_{3-\delta}O_4(111)$ ultrathin films on Pt(111)

P. Morrall,[1] F. Schedin,[1] G. S. Case,[2] M. F. Thomas,[2] E. Dudzik,[3] G. van der Laan,[3] and G. Thornton[1]
[1]*Surface Science Research Centre and Chemistry Department, University of Manchester, Manchester M13 9PL, United Kingdom*
[2]*Department of Physics, Oliver Lodge Laboratory, Oxford Street, University of Liverpool, Liverpool L69 3BX, United Kingdom*
[3]*Magnetic Spectroscopy, Daresbury Laboratory, Warrington WA4 4AD, United Kingdom*
(Received 4 February 2002; revised manuscript received 12 November 2002; published 6 June 2003)

The composition and magnetic properties of two types of ultrathin $Fe_{3-\delta}O_4(111)$ films grown epitaxially on Pt(111) have been characterized using conversion electron Mössbauer spectroscopy (CEMS) and x-ray magnetic circular dichroism (XMCD). CEMS data from both films indicate that the magnetic moments lie in-plane and that a paramagnetic contribution is present that is not seen in spectra of bulk magnetite samples. The XMCD results are in good agreement with theoretical calculations, enabling the stoichiometry of the films to be determined as Fe_3O_4 and $Fe_{2.91}O_4$. The concentrations of both the tetrahedral Fe^{3+} and octahedral Fe^{2+} ions are reduced in the nonstoichiometric film, the decrease in the tetrahedral site probably being due to disorder. CEMS consistently yields a high tetrahedral:octahedral ratio of about 0.7:1, probably because of a contribution from a nonstoichiometric FeO interface layer.

DOI: 10.1103/PhysRevB.67.214408 PACS number(s): 75.50.Gg, 75.70.Ak, 75.70.Rf, 76.80.+y

I. INTRODUCTION

The past decade has seen considerable advances in the study and fabrication of magnetic multilayers and nanostructures. Much of this work has been motivated by interest in spin valves[1] and ferromagnetic tunnel junctions.[2] These systems display large values of magnetoresistance, which can be exploited in devices such as magnetic sensors, read heads for magnetic recording, and nonvolatile magnetic memories.[3,4] Many studies of ferromagnetic tunnel junctions have focused on metallic electrodes separated by an Al_2O_3 barrier. However, ferromagnetic tunnel junctions using an all-oxide structure have recently been shown to exhibit large values of magnetoresistance[5] (MR). These large MR values are almost exclusively obtained at low temperature and/or high magnetic fields although sizable MR has been observed at room temperature for magnetite (Fe_3O_4) nanocontacts.[6]

In principle, Fe_3O_4 is an ideal material for MR applications because of its half metallicity, which theoretically offers an infinite MR ratio.[7,8] Indeed, significant values of spin polarization have been observed for bulk Fe_3O_4 samples.[9–12] However, while epitaxial Fe_3O_4 films have been grown on MgO,[13,14] Al_2O_3,[14–17] and $SrTiO_3$,[18] most studies have focused on films grown on MgO(001) that have exhibited undesired magnetic properties, such as unsaturated magnetization at applied fields as large as 70 kOe.[14] Such undesired properties have been associated with structural defects.[13] In contrast, well-ordered ultrathin epitaxial $Fe_3O_4(111)$ films can be grown on Pt(111),[19–22] and we focus on these films in this study.

Above the Verwey transition temperature[11,23] of Fe_3O_4 at 120 K, the well-known phenomenon of rapid electron hopping creates "$Fe^{2.5+}$" ions and controls the intrinsic electrical properties. The magnetic properties, on the other hand, are known to depend critically on the structural order and stoichiometry. It is therefore imperative that a concise method for determining the structure and stoichiometry of thin films of magnetite is found to enable the development and optimization of iron oxide–based magnetoresistive devices.

Here we present data from two inverse spinel metal oxide ultrathin films, Fe_3O_4 and $Fe_{3-\delta}O_4$, grown on Pt(111). The stoichiometries of the films are obtained using conversion electron Mössbauer spectroscopy (CEMS) and x-ray magnetic circular dichroism (XMCD). This combination is found to be particularly effective. We compare the results from these two techniques in order to demonstrate their potential for determining the quality of iron oxide films. In addition, δ and the ratio of the tetrahedral Fe^{3+}, the octahedral Fe^{2+}, and the octahedral Fe^{3+} ions are all obtained by comparing the XMCD to calculated dichroism spectra.

II. EXPERIMENTAL DETAILS

Iron oxide films were grown on a clean and ordered Pt(111) surface using ^{57}Fe. The base pressure of the growth chamber was 2×10^{-10} mbar. Substrate cleaning employed cycles of 1 keV Ar^+ sputtering and annealing in oxygen at a pressure of 5×10^{-7} mbar and a temperature of 840 K, with subsequent annealing in UHV at 1000 K. This resulted in a clean and ordered Pt(111)1×1 surface as judged by Auger-electron spectroscopy (AES) and low-energy electron diffraction (LEED).

The stoichiometric Fe_3O_4 film was grown by first depositing the equivalent of 6 close-packed monolayers (ML) of high-purity ^{57}Fe at room temperature, with the coverage estimated from AES. It was oxidized for 5 min at an O_2 partial pressure of 1×10^{-6} mbar and a temperature of 830 K. This Fe deposition 830 K oxidation procedure was repeated three times more to form a continuous film. The resulting overlayer is referred to as a 24 ML oxide film by analogy with earlier studies.[19,20] For the nonstoichiometric $Fe_{3-\delta}O_4$ film, a higher O_2 partial pressure of 3×10^{-6} mbar and a higher temperature of 860 K were used to further oxidize the film, while holding all other variables constant. At a thickness of 24 ML, a sharp hexagonal LEED pattern was observed for both films. It was not possible to detect any difference in the

LEED patterns of the two films, which both exhibited a slightly contracted 2×2 periodicity with respect to the substrate, consistent with (111) terminations.[24]

The CEMS and XMCD measurements of the same films were performed *ex situ* without capping the surface. In earlier work, on an 8 ML magnetite film, tests were carried out to investigate the effect of atmospheric contamination, none being found.[25] Changes to neither the structure and cleanliness nor the magnetic hysteresis loops could be detected with LEED, AES, or magneto-optic Kerr effect (MOKE) measurements after a brief exposure of the film to atmosphere. The CEMS spectra were recorded at 293 K in a geometry where the sample surface normal was parallel to the γ-ray beam within a He/CH_4 flow proportional counter. This conventional spectrometer incorporated a 30 mCi ^{57}Co in Rh source and a double-ramp vibration waveform so that the folded spectrum appeared on a flat background. The spectrometer was calibrated using a 25 μm foil of iron, and isomer shift values are quoted relative to Fe at 293 K.

X-ray absorption spectroscopy (XAS) data were recorded using the high-energy spherical grating monochromator beamline 1.1 on the Synchrotron Radiation Source at Daresbury Laboratory using 75% circularly polarized x rays. The sample was mounted on a manipulator inside a small vacuum chamber (10^{-7} mbar) contained between the poles of an electromagnet.[26] The direction of the applied magnetic field was aligned with the x-ray propagation direction, i.e., along the light helicity vector. The sample normal was aligned at an angle of about 45° to the light helicity vector. In this geometry, the in-plane component of the total applied magnetic field of 0.6 T saturates the in-plane magnetization. A much higher field is required to pull the moments out of plane (and align them with the light helicity vector) as evidenced by magnetic hysteresis measurements. The XMCD spectra were corrected for this as well as for the degree of circular polarization. However, it should be pointed out that the scale represents a lower limit of the XMCD signal in the case that the sample would not be completely saturated in the plane. This has no consequences for the XMCD line shape but it scales the absolute signal. The x-ray absorption signal was recorded in the drain current mode and normalized to the incident x-ray flux. The XMCD spectra were obtained by flipping the magnetization direction for each energy point and taking the difference of these simultaneously obtained absorption spectra. All data were recorded at room temperature and the spectra were completely reproducible in repeated scans.

III. THEORY

The theoretical $L_{2,3}$ absorption spectra were calculated using a method described in detail elsewhere.[27] Ground state and final states were calculated at $T=0$ K in intermediate coupling using Cowan's *ab initio* Hartree-Fock code with a relativistic correction. Interatomic screening and mixing were taken into account by reducing the *d-d* and *p-d* Slater integrals with scaling factors $\kappa=0.7$ and 0.8, respectively. For the octahedral sites, a crystal field of $10Dq=1.2$ eV and an exchange field of $\mu_B H=0.01$ eV were used. For the tetrahedral site a crystal field of $10Dq=-0.6$ eV and an exchange field of $\mu_B H=-0.01$ eV were used. The calculated results were broadened by a Lorentzian of $\Gamma=0.3$ (0.5) eV for the L_3 (L_2) edge to account for intrinsic linewidth broadening and a Gaussian of $\sigma=0.25$ eV for instrumental broadening. The main difference between these calculations and those presented by Kuiper *et al.*[28] is our use of a smaller crystal field at the octahedral sites, which leads to slightly better agreement with the experimental results. The relative energies of the calculated spectra for the different Fe sites were shifted to obtain the best fit. Adding them up with a ratio of 1:1:1 gives good agreement with previously reported magnetite film data.[28] The method is very sensitive, and a small change in the site occupancies can give a considerable difference in the relative peak intensities of the XMCD.

In principle, the local ground state at each site is a mixture of different configurations d^n and $d^{n+1}\underline{L}$, where the underscore denotes a hole on the oxygen ligand L.[29] The ground state depends on the *d-L* charge-transfer energy, the *d-d* Coulomb interactions, and the *d-L* mixing (hybridization). The final state in XAS, where an electron has been excited from a $2p$ core level into an empty $3d$ state, is a mixture of the configurations $2\underline{p}3d^{n+1}$ and $2\underline{p}3d^{n+2}\underline{L}$. Hybridization

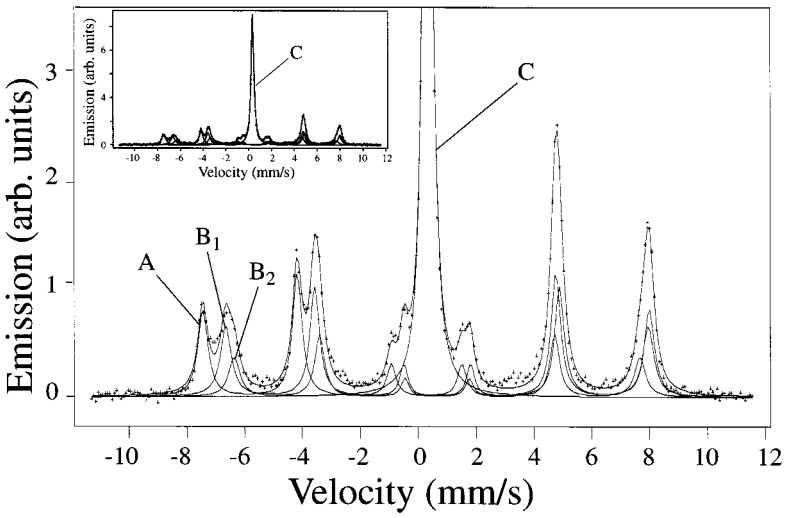

FIG. 1. CEMS spectra recorded at 293 K from a 24 ML film of Fe_3O_4 grown on Pt(111). The full Fe_3O_4 spectrum is shown in the inset. The emission axis zero refers to the fitted background level. Hyperfine parameters of the fitted components are listed in Table I and discussed in the text.

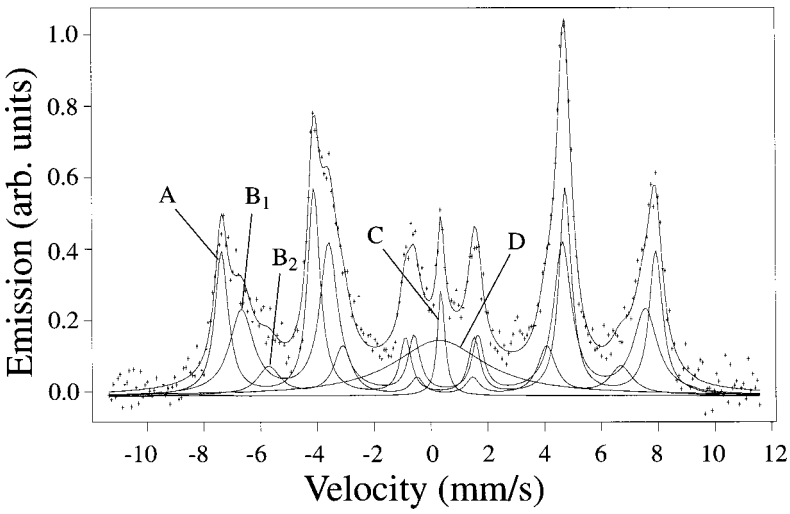

FIG. 2. CEMS spectra recorded at 293 K from 24 ML films of $Fe_{3-\delta}O_4$ grown on Pt(111). The emission axis zero refers to the fitted background level. Hyperfine parameters of the fitted components are listed in Table II and discussed in the text.

mixes both configurations to effectively result in a reduced multiplet width, which can also be interpreted as a reduction of the $2p$-$3d$ exchange interaction due to the delocalization of the valence hole. Since the $2p$-$3d$ and $3d$-$3d$ Coulomb interactions are of similar magnitude, the relative energy positions of the configurations in the initial and final states are also similar. Consequently, the change in hybridization after $2p$ absorption will be small, which results in only a very weak charge-transfer satellite in XAS.

Above the L_3 edge the calculation shows low-intensity multiplet structure that is broadened out in the experimental spectra. This signifies the presence of a charge-transfer satellite. However, it is not meaningful to include the corresponding configuration in the calculation, since this would introduce additional parameters that cannot be determined properly. Therefore, we assume in the treatment of the spectra that each site can be represented by a single configuration with an integer d count. The reduction of multiplet structure arising from configuration mixing can simply be taken into account by scaling the Slater integrals. Such a single-configuration model offers a transparent analysis because the only parameters are the octahedral crystal-field strength $10Dq$ and the scaling factors κ of the Slater integrals.

IV. RESULTS AND DISCUSSION

The CEMS spectra are shown in Figs. 1 and 2, with the hyperfine parameters of the fitted components listed in Tables I and II, respectively. The Fe_3O_4 data in Fig. 1 are seen to be well fitted by three magnetic sextet components and a nonmagnetic singlet, as with our earlier work on an 8 ML film.[24] For the 24 ML film, the magnetic components exhibit hyperfine fields and isomer shifts that are within the range of values reported for bulk Fe_3O_4 at room temperature.[30,31]

Magnetite may be represented as $Fe^{3+}(Fe^{2+}Fe^{3+})O_4$, where the parentheses indicate cations in octahedral (O_h) sites as opposed to tetrahedral (T_d) sites. A schematic of the Fe_3O_4 lattice is shown in Fig. 3. By reference to the interpretation of bulk Fe_3O_4 data,[30,31] the component labeled *A*, in Fig. 1 and Table I, is identified as the Fe^{3+} ion in the tetrahedral site, and those labeled *B* represent a mixture of Fe^{3+} and Fe^{2+} in octahedral lattice sites. B_1 and B_2 are assigned to be inequivalent $Fe^{2.5+}$ ions in the octahedral sites.[25] Although the *B*-site ions are occupied by equal numbers of Fe^{3+} and Fe^{2+} ions, separate patterns are not observed in CEMS due to the fast electron exchange between these cations.[32] Instead, the origin of the two distinct features, B_1 and B_2, arises from the different magnetic dipolar and electric quadrupolar interactions on the inequivalent Fe *B*-site ions, with B_1 and B_2 representing the close-packed and loose-packed octahedral Fe, respectively.[30] The difference between these two types of octahedral Fe layers in the lattice can be seen in Fig. 3. The values of $R=4$ (intensity of lines 2 and 5)/(intensity of lines 3 and 4), where the line numbers are defined from left to right in Fig. 1, for each magnetic sextet component define the spin direction as completely in the plane. These findings are in contrast with the results from Fe_3O_4 films grown on MgO(100),[14] where the

TABLE I. Hyperfine parameters of the fitted components for the Fe_3O_4 CEMS spectra shown in Fig. 1. Errors in parentheses relate to the least significant digit of the value.

Fe_3O_4 components	Isomer shift (mm/s)	Quadrupole splitting (mm/s)	Linewidth (mm/s)	Hyperfine field (kG)	R	Area (%)
A	0.28(1)	−0.02(1)	0.40(1)	478(1)	4.0	24(2)
B_1	0.66(1)	0.00(1)	0.40(1)	452(2)	4.0	22(2)
B_2	0.66(1)	0.00(1)	0.40(1)	434(2)	4.0	12(2)
C	0.35(1)		0.29(1)			42(1)

TABLE II. Hyperfine parameters of the fitted components for the $Fe_{3-\delta}O_4$ CEMS spectra shown in Fig. 2. Errors in parentheses relate to the least significant digit of the value.

$Fe_{3-\delta}O_4$ components	Isomer shift (mm/s)	Quadrupole splitting (mm/s)	Linewidth (mm/s)	Hyperfine field (kG)	R	Area (%)
A	0.30(2)	−0.04(2)	0.52(2)	474(1)	4.0	32(2)
B_1	0.49(3)	−0.08(3)	0.76(3)	440(2)	4.0	36(2)
B_2	0.49(3)	0.00(3)	0.76(3)	384(4)	4.0	11(2)
C	0.37(1)		0.30(1)			3(1)
D	0.29(5)		4.0(5)			18(4)

maximum R value reported ($2p$ in Ref. 14) is 3.2, indicating that the spins are partly out of plane. Moreover, the relative occupancy of the A (tetrahedral) and B (octahedral) sites is $0.71 \pm 0.1{:}1$ in our ultrathin Fe_3O_4 film, whereas it is 0.5:1 in the thicker films formed in Ref. 14 and in bulk Fe_3O_4.[30,31]

Oxidized Fe_3O_4 films have a stoichiometry between that of magnetite and maghemite (γ-Fe_2O_3) and can be represented as $Fe^{3+}(Fe^{2+}_{1-3\delta}Fe^{3+}_{1+2\delta}X_\delta)O_4$, where X represents vacancies in the octahedral sites. δ lies in the range $0-\frac{1}{3}$, corresponding to magnetite and maghemite, respectively. The $Fe_{3-\delta}O_4$ CEMS data shown in Fig. 2 are fitted by three magnetic sextet components, a nonmagnetic singlet, and a further undefined contribution D. The linewidths in the $Fe_{3-\delta}O_4$ spectrum are significantly greater than those in the Fe_3O_4 spectrum. This suggests that the film is not as well ordered, which may also be the origin of the extra component D in the fit. Line D, which is observed in Fig. 2 but has not been observed in films oxidized at 830 K has an isomer shift characteristic of Fe^{3+} and a width consistent with a distribution of hyperfine fields. A possible cause of such a feature is superparamagnetic grains (of Fe_3O_4 or γ-Fe_2O_3), which interacts to smear out the magnetic hyperfine interaction. Such a component is separate from crystalline Fe_3O_4, which composes ~80% of the spectrum and is analyzed separately.

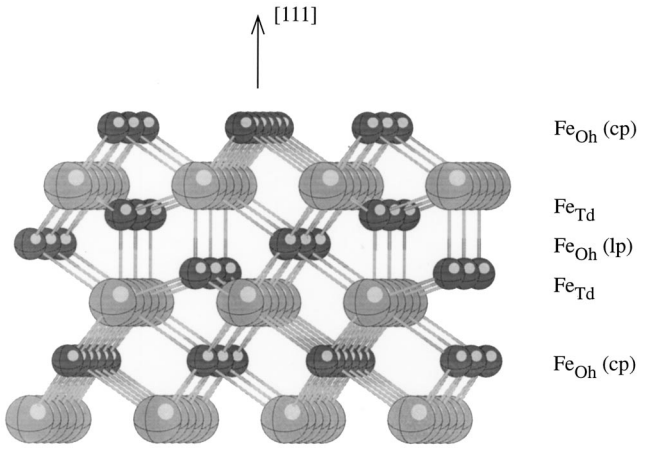

FIG. 3. Schematic diagram of the Fe_3O_4 lattice. Successive Fe ion layers exist along the [111] direction. The three basic types of Fe layers, close-packed octahedral, Fe_{O_h}(cp), tetrahedral, Fe_{T_d}, and loose-packed octahedral, Fe_{O_h}(1p), are indicated. The remaining layers consist of close-packed oxygen.

The A-site magnetic components exhibit hyperfine fields and isomer shifts that are still within the range of values reported for bulk Fe_3O_4 at room temperature.[30,31] However, the isomer shifts for the B sites in the $Fe_{3-\delta}O_4$ film indicate a charge state somewhere between $Fe^{2.5+}$ and Fe^{3+}. This is consistent with the model $Fe^{3+}(Fe^{2+}_{1-3\delta}Fe^{3+}_{1+2\delta}X_\delta)O_4$, where as δ increases the B-site charge state also increases from 2.5+ for Fe_3O_4 to 3+ for γ-Fe_2O_3. As also found for the Fe_3O_4 film, the values of $R=4$ for each magnetic sextet component define the spin direction as completely in the plane. The CEMS data for the $Fe_{3-\delta}O_4$ film somewhat surprisingly indicate that the relative occupancy of the A and B sites is $0.68 \pm 0.1{:}1$, which is close to, but smaller than, the ratio found for the Fe_3O_4 film. Intuitively, the $A{:}B$ ratio would be expected to increase as δ increases and as the number of B-site ions decreases. We address this issue below in the context of the XMCD results.

One explanation for the increased $A{:}B$ ratio found in CEMS for both films could be a contribution from a layer with FeO stoichiometry at the Fe_3O_4/Pt interface.[24] Such a layer is not unexpected on the basis of work that showed that the first 1–2 ML of Fe_3O_4 films on Pt(111) grow as FeO.[33] Work by Dimitrov *et al.*[34] has suggested that FeO films that are nonstoichiometric, i.e., $Fe_{1-x}O$, tend to form clusters of tetrahedrally coordinated Fe^{3+} ions in an environment very similar to that of Fe_3O_4. In our films it is very probable that the FeO layer would be nonstoichiometric, as the growth conditions used are designed to suit Fe_3O_4 rather than FeO film growth. If tetrahedrally coordinated Fe^{3+} ions exist in the FeO layer, then it may not be possible to observe them as a separate signal using CEMS since their environment would be similar to that of the Fe_3O_4 A-site contributions, and their magnetic moments would be coupled to that of the rest of the film. Hence, they would appear as part of the overall Fe^{3+} A-site contribution and increase the $A{:}B$ ratio.

The nonmagnetic singlet component C, seen in the inset of Fig. 1 and in Fig. 2, is not seen in CEMS spectra of bulk Fe_3O_4. In earlier work with an 8 ML Fe_3O_4 film, we concluded that the equivalent peak arose from an FeO interface layer on the basis of its area ratio. A paramagnetic signature for such a layer was considered likely because the measurement temperature was above the Néel temperature for FeO. However, further spectra have revealed that the paramagnetic feature C arises from Fe diffused into the Pt substrate. The isomer shift for this single line in our spectra is 0.35 ± 0.01 mm/s, which is in exact agreement with the value of

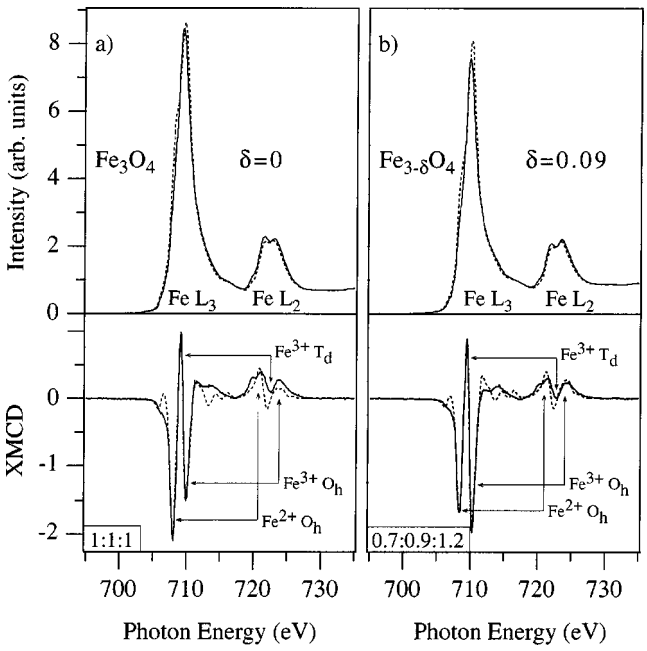

FIG. 4. X-ray absorption spectra for (a) Fe_3O_4 and (b) $Fe_{3-\delta}O_4$ grown on Pt(111) recorded with left- and right-handed circularly polarized light (solid and dotted line). The bottom panels show the XMCD spectra with experimental results given as a solid line and calculated results as a dashed line. The XAS spectra are shown as raw data, while the XMCD data have been corrected for the sample geometry and beam polarization. The insets show the relative ratio of the ions of the calculated dichroism, in the order $Fe_{O_h}{}^{2+}$:$Fe_{T_d}{}^{3+}$:$Fe_{O_h}{}^{3+}$, each normalized to the value for stoichiometric Fe_3O_4. The same arbitrary units are used for the scale in both the XAS and XMCD data.

0.349 ± 0.006 mm/s for Fe diffused into Pt.[35] This latter value is accurately known as some Mössbauer sources use Pt as a matrix for the diffused ^{57}Co (^{57}Fe). The large difference in intensity of line *C* in Figs. 1 and 2 arises from the fact that in Fig. 1 the substrate had a previous history of ^{57}Fe deposition at 830 K.

Further information can be extracted from the CEMS data by comparing the spectra for the two films. Since the technique can differentiate between the two inequivalent Fe *B* sites, it should to some extent be possible to draw conclusions about where the *B* site vacancies occur in nonstoichiometric films. As mentioned above, B_1 relates to the Fe sites that are close-packed octahedral and B_2 to loose-packed octahedral sites.[30] In bulk magnetite the ratio $B_1:B_2$ is 3:1. In our more oxidized film the $B_1:B_2$ occupancy ratio appears higher than that in our stoichiometric film, suggesting that the Fe vacancies in the $Fe_{3-\delta}O_4$ film are located predominantly in the loose-packed octahedral layer.

Turning to the XMCD results, Fig. 4 (top panels) shows the Fe $2p$ XAS data for the 24 ML Fe_3O_4 and $Fe_{3-\delta}O_4$ films with parallel and antiparallel alignments of the light helicity vector to the projected component of sample magnetization. Reversal of the magnetization has the same effect as reversal of the light helicity vector. The XMCD spectra are shown in the bottom panels of Fig. 4, where the dashed lines indicate the calculated dichroism. The XMCD signal is characterized by three contributions. In accordance with earlier reports, the contribution from Fe^{2+} and Fe^{3+} spin-up ions on octahedral sites are seen as negative peaks at the Fe L_3 absorption edge and positive peaks in the Fe L_2 edge.[28] The octahedral Fe ions are distinguished by their oxidation state in XMCD because of the shorter time scale of the spectroscopy compared with CEMS. The Fe^{3+} spin-down ions on tetrahedral sites are seen as a positive peak at the Fe L_3 edge and a negative peak at the Fe L_2 edge.[28] The inset (bottom panels) shows the relative intensities of the three contributions found by fitting the calculated spectra to the experimental data. These relative intensities are given with respect to pure magnetite; this is the reason why the $Fe_{O_h}{}^{3+}$ contribution exceeds a value of 1 for the $Fe_{3-\delta}O_4$ film. Spectrum fitting was restricted to the L_3 dichroism peaks since a fit over the full energy range provides less accurate results. This arises in part because the appearance of the L_2 edge can be changed by the Coster-Kronig interaction between the discrete states $2p_{1/2}3d^n$ and continuum states $2p_{3/2}3d^{n-1}k$, where k is a continuum electron. Moreover, the theoretical model employed does not describe the region between L_3 and L_2 particularly well, since configurations that are higher in energy are neglected. This probably gives rise to the discrepancies between theory and experiment observed in this region of the spectra.

The XMCD calculations agree well with the Fe_3O_4 data, the best fit resulting in a 1:1:1 ratio for $Fe_{O_h}{}^{2+}$:$Fe_{T_d}{}^{3+}$:$Fe_{O_h}{}^{3+}$, giving $\delta=0$ and an $A:B$ ratio of 0.50:1, found by solving for δ in $Fe^{3+}(Fe_{1-3\delta}{}^{2+}Fe_{1+2\delta}{}^{3+}X_\delta)O_4$. If the same fitting procedure is used for the $Fe_{3-\delta}O_4$ data, the ratio for $Fe_{O_h}{}^{2+}$:$Fe_{T_d}{}^{3+}$:$Fe_{O_h}{}^{3+}$ is found to be 0.7:0.9:1.2, giving $\delta=0.09$, which would lead to a theoretical $A:B$ ratio of 0.52:1. Inspection of the two dichroism data sets in Fig. 4 reveals that in the $Fe_{3-\delta}O_4$ film the $Fe_{O_h}{}^{2+}$ contribution is reduced as expected compared to the Fe_3O_4 film. However, our experimentally derived $A:B$ ratios for the Fe_3O_4 and $Fe_{3-\delta}O_4$ films give 0.50 and 0.49, respectively. Again, as with the CEMS data, the ratio does not change as expected for a reduction in the $Fe_{O_h}{}^{2+}$ contribution. The dichroism data provide an explanation for this apparent discrepancy. While the $Fe_{O_h}{}^{2+}$ peak is reduced, so too is the $Fe_{T_d}{}^{3+}$ peak, which is impossible to detect from the CEMS data where we are looking at ratios rather than absolute values of the site occupancy. An ideal $Fe_{3-\delta}O_4$ film would have the relative size of the $Fe_{T_d}{}^{3+}$ peak as 1, not 0.9 as in our case, which appears to be due to a less-ordered structure for the nonstoichiometric film. The relative site occupancies from the two techniques are summarized in Table III.

Our experimental results are largely consistent with an earlier XMCD study of $Fe_{3-\delta}O_4$(100)/MgO(100) films with values covering the full range of δ.[36] There are two differences, however, one being that our Fe_3O_4 film appears to have a larger $Fe_{O_h}{}^{2+}$ contribution. When the Fe_3O_4 film in Ref. 36 is compared to our theoretical calculations, a δ of approximately 0.03 is found, suggesting that the nominally Fe_3O_4 film in the earlier work was in fact slightly oxidized.

TABLE III. Relative site occupancies deduced from CEMS and XMCD spectra. The $Fe_{O_h}{}^{2+}$:$Fe_{T_d}{}^{3+}$:$Fe_{O_h}{}^{3+}$ ratio from the XMCD data is defined as relative to pure Fe_3O_4. The error in the XMCD site ratios are estimated to be $\pm 3\%$.

	CEMS		XMCD	
	$A:B$	$B_1:B_2$	$A:B$	$Fe_{O_h}{}^{2+}$:$Fe_{T_d}{}^{3+}$:$Fe_{O_h}{}^{3+}$
Fe_3O_4	0.71 ± 0.1	1.83	0.50	1.0:1.0:1.0
$Fe_{3-\delta}O_4$	0.68 ± 0.1	3.27	0.49	0.7:0.9:1.2

A second difference is that our $Fe_{3-\delta}O_4$ data seem to have a smaller $Fe_{T_d}{}^{3+}$ contribution compared to the equivalent data in Ref. 36. This is in line with the $A:B$ ratio determined by XMCD for our nonstoichiometric film, being slightly smaller than expected.

Another study reported XMCD data from an $Fe_3O_4(111)/Fe(110)/W(110)$ system during various stages of oxidation.[37] The results in Ref. 37 include data from the final stage of oxidation to $Fe_3O_4(111)$ of an Fe(110) film with an XMCD spectrum essentially identical to our data for the stoichiometric Fe_3O_4 film. The earlier report relies on an accurate subtraction of the signal from the underlying Fe metal layer and an amount that is concluded to be paramagnetic FeO or other departures from Fe_3O_4 stoichiometry at the film interface. We point out here that such contributions would easily be deduced from CEMS data for the same film. This further shows the usefulness of comparing the two techniques in the characterization of the stoichiometry and composition of iron oxide films.

If we compare our CEMS and XMCD results, we can see that they are consistent if we take into account the sampling depth of the two techniques. CEMS samples the complete 24 ML film, whereas the drain current measurement of XMCD is surface sensitive. Hence, the FeO interface that we suggest causes the $A:B$ (terahedral:octahedral) ratio to be about 0.7 in CEMS for both films is not detected by XMCD, leading to the expected ratio of about 0.5. The two techniques are also seen to be complementary. CEMS gives a measure of the quality of the films through the observed linewidths. It also reveals information about the orientation of the magnetic moments for each contribution in the spectra and about the individual B_1 (close-packed octahedral) and B_2 (loose-packed octahedral) site ratios. XMCD, on the other hand, can determine the concentration of $Fe_{T_d}{}^{3+}$, $Fe_{O_h}{}^{2+}$, and $Fe_{O_h}{}^{3+}$ relative to the stoichiometric Fe_3O_4 film. This allows δ to be determined for $Fe_{3-\delta}O_4$, as well as the $A:B$ ratio.

V. SUMMARY

Stoichiometry is of paramount importance in thin Fe_3O_4 films for controlling the electric and magnetic properties and even changes in composition occurring deep in the film can in turn affect the surface magnetic properties. Here a comparison has been made between CEMS and XMCD data with the aim to show the power of these techniques in confirming overall film and surface stoichiometry. With the aid of magnetic information, contributions to the spectra can be resolved that remain unresolved with more conventional techiques, such as x-ray photoelectron spectroscopy. Thin films of Fe_3O_4 and $Fe_{3-\delta}O_4$ have been produced, both of which exhibit evidence of a spontaneous and complete in-plane ferrimagnetic alignment of magnetic moments. CEMS has been used to show that the stoichiometric film exhibits isomer shifts and hyperfine fields in line with that of bulk Fe_3O_4. Furthermore, the isomer shifts in CEMS indicate a charge state of $+2.5$ on the O_h Fe sites, which is expected for the stoichiometric film, whereas for the nonstoichiometric film a higher charge state is found, indicating a tendency towards γ-Fe_2O_3. There is some evidence in the CEMS data for $Fe_{3-\delta}O_4$ that Fe *B*-site vacancies occur predominantly at the loose-packed octahedral layers. A paramagnetic contribution seen in CEMS from magnetite films grown on Pt(111) is thought to originate from Fe dissolved in the substrate lattice. CEMS data indicate a tetrahedral to octahedral site ratio of about 0.7 for both films, compared to an expected value of 0.5, which probably arises from *A*-site-like contributions from a non-stoichiometric interface layer of FeO.

XMCD data exhibit characteristic contributions from Fe^{3+} ions in tetrahedral sites and Fe^{2+} and Fe^{3+} ions in octahedral sites, which can largely be resolved separately. Good agreement is demonstrated between the XMCD experimental data and theoretical calculations, confirming the quality of the films and enabling the determination of δ for the Fe_3O_4 ($\delta=0.00$) and the $Fe_{3-\delta}O_4$ ($\delta=0.09$) films. The relative occupancy of tetrahedral and octahedral sites derived from XMCD is 0.5 for the stoichiometric film, as expected, differing from the CEMS value because of its different sampling depth. The concentrations of both the tetrahedral Fe^{3+} and octahedral Fe^{2+} ions are reduced in the nonstoichiometric film, the decrease in the tetrahedral site probably being due to disorder. This is consistent the CEMS data, which evidence a degree of disorder through an increased linewidth.

ACKNOWLEDGMENT

This work was funded by the EPSRC (U.K.).

[1] G. A. Prinz, Science (Washington, DC, U.S.) **282**, 1660 (1998).
[2] J. S. Moodera, L. R. Kinder, T. M. Wong, and R. Meservey, Phys. Rev. Lett. **74**, 3273 (1995).
[3] G. A. Prinz, Phys. Today **48** (4), 58 (1995).
[4] J. Gregg, W. Allen, N. Viart, R. Kirschman, C. Sirisathitkul, J. P. Schille, M. Gester, S. Thompson, P. Sparks, V. DaCosta, K. Ounadjela, and M. Skvarla, J. Magn. Magn. Mater. **175**, 1 (1997).
[5] K. Ghosh, S. B. Ogale, S. P. Pai, M. Robson, E. Li, I. Jin, Z. Dong, R. L. Greene, R. Ramesh, and T. Venkatesan, Appl. Phys. Lett. **73**, 689 (1998).
[6] J. J. Versluijs and J. M. D. Coey, J. Magn. Magn. Mater. **226–230**, 688 (2001).
[7] A. Yanase and K. Siratori, J. Phys. Soc. Jpn. **53**, 312 (1984).

[8] Z. Zhang and S. Satpathy, Phys. Rev. B **44**, 13 319 (1991).
[9] A. M. Bratkovsky, Appl. Phys. Lett. **72**, 2334 (1998).
[10] R. Meservey and P. M. Tedrow, Phys. Rep. **238**, 173 (1994).
[11] E. J. W. Verwey and P. W. Haayman, Physica (Amsterdam) **VIII**(9), 979 (1941).
[12] A. Kozlowski, R. J. Rasmussen, J. E. Sabol, P. Metcalf, and J. M. Honig, Phys. Rev. B **48**, 2057 (1993), and references therein.
[13] D. T. Margulies, F. T. Parker, M. L. Rudee, F. E. Spada, J. N. Chapman, P. R. Aitchison, and A. E. Berkowitz, Phys. Rev. Lett. **79**, 5162 (1997).
[14] D. T. Margulies, F. T. Parker, F. E. Spada, R. S. Goldmann, J. Li. R. Sinclair, and A. E. Berkowitz, Phys. Rev. B **53**, 9175 (1996).
[15] T. Fujii, M. Takano, R. Katano, Y. Isozumi, and Y. Bando, J. Magn. Magn. Mater. **130**, 267 (1994).
[16] S. Gota, E. Guiot, M. Henriot, and M. Gautier-Soyer, Surf. Sci. **454–456**, 796 (2000).
[17] C. A. Kleint, H. C. Semmelhack, M. Lorenz, and M. K. Krause, J. Magn. Magn. Mater. **140–144**, 725 (1995).
[18] W. F. J. Fontijn, R. M. Wolf, R. Metselaar, and P. J. van der Zaag, Thin Solid Films **292**, 270 (1997).
[19] W. Weiss, A. Barbieri, M. A. van Hove, and G. A. Somorjai, Phys. Rev. Lett. **71**, 1848 (1993).
[20] A. Barbieri, W. Weiss, M. A. van Hove, and G. A. Somorjai, Surf. Sci. **302**, 259 (1994).
[21] H. C. Galloway, J. J. Benitez, and M. Salmeron, Surf. Sci. **298**, 127 (1993).
[22] Y. J. Kim, C. Westphal, R. X. Ynzunza, H. C. Galloway, M. Salmeron, M. A. Van Hove, and C. S. Fadley, Phys. Rev. B **55**, R13 448 (1997).
[23] F. Walz, J. Phys.: Condens. Matter **14**, R285 (2002).
[24] F. Schedin, L. Hewitt, P. Morrall, V. N. Petrov, G. Thornton, S. Case, M. F. Thomas, and V. M. Uzdin, Phys. Rev. B **58**, R11 861 (1998).
[25] F. Schedin, P. Morrall, V. N. Petrov, S. Case, M. F. Thomas, E. Dudzik, G. van der Laan, and G. Thornton, J. Magn. Magn. Mater. **211**, 266 (2000).
[26] E. Dudzik, G. van der Laan and S. M. Thompson, Synchrotron Radiat. News **13**, 18 (2000).
[27] G. van der Laan and B. T. Thole, Phys. Rev. B **43**, 13 401 (1991).
[28] P. Kuiper, B. G. Searle, L. C. Duda, R. M. Wolf, and P. J. van der Zaag, J. Electron Spectrosc. Relat. Phenom. **86**, 107 (1997).
[29] G. van der Laan, J. Zaanen, G. A. Sawatzky, R. C. Karnatak, and J. M. Esteva, Phys. Rev. B **33**, 4253 (1986).
[30] L. Häggström, H. Annersten, T. Ericsson, R. Wäppling, W. Karner, and S. Bjarman, Hyperfine Interact. **5**, 201 (1978).
[31] E. De Grave, R. M. Persoons, R. E. Vandenberghe, and P. M. A. de Bakker, Phys. Rev. B **47**, 5881 (1993), and references therein.
[32] G. M. Da Costa, E. De Grave, P. M. A. De Bakker, and R. E. Vandenberghe, Clays Clay Miner. **43**, 656 (1995).
[33] M. Ritter, W. Ranke, and W. Weiss, Phys. Rev. B **57**, 7240 (1998).
[34] D. V. Dimitrov, G. C. Hadjipanayis, V. Papaefthymiou, and A. Simopoulos, J. Vac. Sci. Technol. A **15**, 1473 (1997).
[35] S. M. Qaim, Proc. Phys. Soc. London **90**, 1065 (1967).
[36] E. Pellegrin, M. Hagelstein, S. Doyle, H. O. Moser, J. Fuchs, D. Vollath, S. Schuppler, M. A. James, S. S. Saxena, L. Niesen, O. Rogojanu, G. A. Sawatzky, C. Ferrero, M. Borowski, O. Tjernberg, and N. B. Brookes, Phys. Status Solidi B **215**, 797 (1999).
[37] H.-J. Kim, J.-H. Park, and E. Vescovo, Phys. Rev. B **61**, 15 284 (2000).